Time-evolution operator method for non-Markovian density matrix propagation in time and space representation: Application to laser association of OH in an environment

G. K. Paramonov[1] and Peter Saalfrank[2]

[1]*Institute of Physics, National Academy of Sciences of Belarus, Independence Avenue 70, 220602 Minsk, Republic of Belarus*
[2]*Institut für Chemie, Universität Potsdam, Karl-Liebknecht-Strasse 24-25, D-14476 Potsdam-Golm, Germany*

An efficient method for the numerical solution of a non-Markovian, open-system density matrix equation of motion in coordinate representation is developed. We apply the scheme to model simulations of the laser-assisted O+H→OH association reaction in an environment. The suggested approach is based on the application of the time-evolution operator to the "closed-system" part of the overall Hamiltonian and transformation of the open-system equation of motion to the Heisenberg picture suitable for numerical propagation. A dual role of the system-environment coupling with respect to the infrared (ir) laser-driven association of OH is demonstrated: the association probability is increased due to the coupling at relatively weak laser fields, but decreased at strong laser fields. Moreover, at a certain strength of the ir laser field, the association probability does not depend on the strength of the system-bath coupling at all.

I. INTRODUCTION

Photoassociation reactions, wherein two colliding atoms interact with an external laser field to form a bound molecular state, has attracted much attention in the past [1–14] and more recently [15–21]. Especially promising is a growing trend to investigate photoassociation reactions in the time domain [3,7–12,14–16,18–21], which makes it possible to employ laser-field optimization and control techniques. Until now theoretical investigations of the laser-driven quantum dynamics of two colliding atoms have been performed within the time-dependent Schrödinger wave-function formalism [8,10–12,14–16,18–21], including the optimal control of vibrationally state-selective photoassociation in the ground electronic state,

$$A + B \rightarrow AB(v), \tag{1}$$

with shaped ir laser pulses [8,11,18,19].

In the present work we study the quantum dynamics of association reaction (1) in an environment. Since in this case a wave-function approach, i.e., solution of the time-dependent Schrödinger equation for the full system plus environment, is possible only for model problems (see, e.g., [22] for the example of laser-free gas-surface scattering), we use open-system density matrix theory here. For this purpose we extend the previously used numerical methods [30,31], i.e., the time-dependent, reduced non-Markovian density matrix formalism in the state representation, to the coordinate representation. This is the natural choice for a problem including unbound motion. Specifically, we investigate the central collision of O and H atoms, which takes place in an environment treated as an unobserved "bath." Interaction of the "O+H" system with the bath results in the formation of OH in the case of laser-free collisions. We also investigate the vibrationally state-selective photoassociation of OH controlled by ir laser pulses. In the latter case, the system-bath coupling facilitates stabilization of OH due to relaxation to the lower-lying vibrational states.

In our previous works [30,31] the non-Markovian laser-driven dissipative dynamics of OH was treated in the state representation, including the discretization of unbound continuum states, for bound-bound and bound-continuum transitions only, while the continuum-continuum transitions were not taken into account therein. In contrast, the numerical methods developed in the present work for the coordinate representation allow unbound systems to be treated explicitly.

Note that association reactions in an environment are also most relevant for gas-surface scattering. Then the collision partners are an atom or molecule and a surface, and association is called sticking or adsorption. In this case the effects of dissipation are coordinate dependent, typically increasing toward the surface. Dissipative gas-surface scattering with and without support of a laser has been studied quantum mechanically in the past [22–26]. Also the reverse process to association, sticking, or adsorption, namely, the desorption of adspecies from substrates, has been studied [27–29]. In many of the above examples, open-system density matrix theory was used. In these cases, in addition to the "reduced" approach, at least one of the following two approximations was made additionally: (1) The unbound continuum was discretized by quasibound states and/or (2) the dynamics was Markovian, i.e., memory effects were neglected. This is where the present study tries to go beyond the previous work.

In more practical terms, we want to address the questions as to how the association probability depends on the system-bath coupling parameters, and on the ir field if one is applied. The matter-field interaction is treated semiclassically, with the electric field determined from the vector potential to satisfy Maxwell's equations.

The paper is organized as follows. The model for association of O and H in an environment and the numerical techniques used are described in Sec. II. The quantum dynamics of the laser-free and the laser-driven association is presented in Sec. III. The results obtained are summarized and discussed in the concluding section.

II. MODEL EQUATIONS OF MOTION AND TECHNIQUES

The model used is this study is based on the previous work [8,11,30,31]. The total Hamiltonian $\hat{H}_T$ is divided into four parts,

$$\hat{H}_T(r,\{z_u\},t) = \hat{H}_S(r) + \hat{H}_{SF}(r,t) + \hat{H}_{SB}(r,\{z_u\}) + \hat{H}_B(\{z_u\}),$$
(2)

where $\hat{H}_S(r)$ represents the O+H system, $\hat{H}_{SF}(r,t)$ describes the interaction of the system and the laser field, $\hat{H}_{SB}(r,\{z_u\})$ describes the system-bath interactions, and $\hat{H}_B(\{z_u\})$ represents the bath, where $\{z_u\}$ stands for the bath degrees of freedom. Atomic units are used below unless otherwise explicitly indicated.

As possible concrete applications of this model we have in mind the laser-induced formation of an O-H bond at a solid (oxide) or a liquid (water) surface, or the same process in a liquid or an inert solid environment such as a rare gas matrix. In these cases the environmental modes are phonons or low-amplitude motions of solvent molecules, respectively.

The system Hamiltonian is given as in previous works [8,11,30,31] by

$$\hat{H}_S(r) = \frac{\hat{p}^2}{2m} + V_M(r),$$
(3)

where r is the internuclear distance and m is the reduced mass of the O and H atoms: $m=1728.538 m_e$, where m_e stands for the electron rest mass. In Eq. (3), $V_M(r)$ stands for the Morse potential for the electronic ground state of OH supporting 22 bound vibrational states,

$$V_M(r) = D_e\{\exp[-\beta(r-r_e)] - 1\}^2 - D_e,$$
(4)

with the well depth $D_e=0.1994 E_H$, the equilibrium bond length $r_e=1.821 a_0$, and the Morse parameter $\beta=1.189 a_0^{-1}$ (E_H is the Hartree energy, and a_0 is the Bohr radius).

The interaction of the O+H system with a laser field, which is assumed to be linearly polarized along the O-H axis, is treated within the semiclassical electric dipole approximation by the Hamiltonian

$$\hat{H}_{SF}(r,t) = \frac{\mu(r)}{c} \frac{\partial A(t)}{\partial t},$$
(5)

where $A(t)$ is the vector potential, c is the speed of light, and the dipole moment operator $\mu(r)$ is given by the Mecke function

$$\mu(r) = -q_\mu r \exp(-r/r_\mu),$$
(6)

with $q_\mu=1.634|e|$ and $r_\mu=1.134 a_0$.

The initial state of the O+H system is a free state of O and H atoms in the energy continuum. It is represented as in [8,11,19] by a Gaussian wave packet,

$$\Psi(r,t=0) = \left(\frac{2}{\pi\Delta^2}\right)^{1/4} \exp\left[ik_0 r - \left(\frac{r-r_0}{\Delta}\right)^2\right],$$
(7)

where $\Delta=9.675 a_0$ is the width of the wave packet (7), the average initial internuclear distance is $r_0=31.01 a_0$, and the

relative momentum is $\hbar k_0$ with $k_0=-3.5 a_0^{-1}$. Accordingly, the density matrix at $t=0$ is written as follows:

$$\sigma(r,r',t=0) = \Psi^*(r',t=0)\Psi(r,t=0).$$
(8)

In a certain domain of the internuclear distance, $r < r_B$, the O+H system interacts with an unobserved quasiresonant bath. The system-bath interaction Hamiltonian $\hat{H}_{SB}(r,\{z_u\})$ is taken as in [30,31] in the following form:

$$\hat{H}_{SB}(r,\{z_u\}) = \Lambda Q(r) F(\{z_u\}),$$
(9)

where Λ is a coupling constant that measures the overall strength of the system-bath coupling, while $Q(r)$ and $F(\{z_u\})$ are the system and the bath coupling operators, respectively.

The system coupling operator $Q(r)$ is modified from [30,31] as follows:

$$Q(r) = \begin{cases} (1/\beta)\{1 - \exp[-\beta(r-r_e)]\} & \text{for } r \leq r_1, \\ Q(r_1)\cos^2\left[\frac{\pi}{2}\left(\frac{r-r_1}{r_B-r_1}\right)\right] & \text{for } r_1 \leq r \leq r_B, \\ 0 & \text{for } r > r_B. \end{cases}$$
(10)

The value of $Q(r_1)$ in the second line of Eq. (10) is calculated from the first line therein at $r=r_1$, and r_1 is always chosen such that $Q(r_1) \simeq 1$. By the choice (10), we assume a coordinate-dependent coupling which goes smoothly to zero for large r. Numerical parameters r_1 and r_B, defining the various regions of Q, are chosen as follows: $r_1=12 a_0$ and $r_B=20 a_0$. The $\cos^2$ function used in the second line of Eq. (10) to accomplish a smooth transition from $Q(r) \simeq 1$ at $r=r_1$ to $Q(r)=0$ at $r \geq r_B$ out of the interaction domain is rather arbitrary. Of course, other choices of the coordinate dependence of $Q(r)$ are also possible.

The bath coupling operator $F(\{z_u\})$ is assumed to be linear and factorized with respect to the bath degrees of freedom as in [30,31]:

$$F(\{z_u\}) = \sum_u K_u z_u, \quad u=1,2,\ldots.$$
(11)

This is a good approximation if one assumes only small displacements of the bath modes during the association process.

The bath is treated as an infinite ensemble of harmonic oscillators and represented by the Hamiltonian

$$\hat{H}_B(\{z_u\}) = \sum_u \frac{\hat{p}_u^2}{2m_u} + \frac{m_u}{2} \Omega_u^2 z_u^2,$$
(12)

where m_u is the mass and Ω_u is the frequency of the bath oscillator u. The eigenfunctions of the bath degrees of freedom are the well-known harmonic oscillator wave functions.

The density matrix equation of motion used below is derived as follows. We start with the Liouville equation [32] for the density matrix $\sigma(t)$ of the total system in the Schrödinger picture,

$$i\hbar\frac{\partial\sigma(t)}{\partial t} = [\hat{H}_T(t), \sigma(t)],\tag{13}$$

and transform it into the interaction picture with respect to the bath degrees of freedom only,

$$\sigma_I(t) = \exp(i\hat{H}_B t/\hbar)\sigma(t)\exp(-i\hat{H}_B t/\hbar).\tag{14}$$

The resulting equation of motion can be written as follows:

$$i\hbar\frac{\partial\sigma_I(t)}{\partial t} = [\hat{H}_S, \sigma_I(t)] + [\hat{H}_{SF}(t), \sigma_I(t)]$$
$$+ \Lambda[Q(r)F_I(\{z_u\}), \sigma_I(t)],\tag{15}$$

where the bath coupling operator in the interaction picture reads

$$F_I(\{z_u\}, t) = \exp(i\hat{H}_B t/\hbar)F(\{z_u\})\exp(-i\hat{H}_B t/\hbar),\tag{16}$$

while the other operators of Eq. (13) are not affected by the transformation (14).

In the next step, the time-evolution operator $S(r,r',t)$ is employed in Eq. (15) to transform it to the Heisenberg picture with respect to the system coordinate r as follows:

$$\sigma_I(t) = S(t)\sigma_H(t)S(t)^{-1},\tag{17}$$

where $\sigma_H(t)$ is the density matrix of the total system in the Heisenberg picture, and $S(r,r',t)$ is the time-evolution operator in the Schrödinger picture, satisfying the equation of motion

$$i\hbar\frac{\partial S(t)}{\partial t} = \hat{H}_S(r)S(t) + \hat{H}_{SF}(r,t)S(t)\tag{18}$$

and the initial conditions

$$S(r,r',t=0) = \hat{1},\tag{19}$$

where $\hat{1}$ is the unit operator, and $S(t)S^{-1}(t) = \hat{1}$ at any time t. Note that the inverse operator $S^{-1}(t)$ is not equal to the Hermitian conjugate of $S(t)$ if imaginary absorbing boundaries are employed (see below).

Substituting Eq. (17) into Eq. (15) and taking into account Eq. (18), we finally get the equation of motion in the Heisenberg picture,

$$i\hbar\frac{\partial\sigma_H(t)}{\partial t} = \Lambda[Q_H(r,r',t)F_I(\{z_u\},t), \sigma_I(t)],\tag{20}$$

where $Q_H(r,r',t)$ is the system coupling operator in the Heisenberg picture,

$$Q_H(r,r',t) = S^{-1}(r,r',t)Q(r)S(r,r',t).\tag{21}$$

It also follows from Eqs. (14), (17), and (19) that initially, at $t=0$, when the O+H system is far from the interaction domain,

$$\sigma_H(r,r',t=0) = \sigma(r,r',t=0),\tag{22}$$

where $\sigma(r,r',t=0)$ is given by Eq. (8). Note that Eq. (20) is still exact.

The statistical description of the O+H system coupled to an unobserved bath is made by the reduced density matrix $\rho_H(r,r',t)$, which is defined as

$$\rho_H(r,r',t) = \mathrm{Tr}_B[\sigma(r,r',\{z_u\},t)],\tag{23}$$

where Tr_B refers to the trace over all degrees of freedom of the bath $\{z_u\}$. The equation of motion for the reduced density matrix $\rho_H(t)$ is obtained as in [32] by making use of the formal solution of Eq. (20),

$$\sigma_H(t) = \sigma_H(0) - \frac{i}{\hbar}\Lambda\int_0^t dt'[Q_H(t')F_I(t'), \sigma_H(t')],\tag{24}$$

substituting it back into Eq. (20), and evaluating the trace (23) under the basic condition of irreversibility, $\sigma_H(t) = \rho_H(t)\rho_B(0)$, where

$$\rho_B(0) = \exp(-\hat{H}_B/k_B T)/\mathrm{Tr}_B[\exp(-\hat{H}_B/k_B T)].\tag{25}$$

The final equation of motion for the reduced density matrix in the Heisenberg picture reads

$$\frac{\partial\rho_H(t)}{\partial t} = -\left(\frac{\Lambda}{\hbar}\right)^2[Q_H(r,r',t), G_H(r,r',t)],\tag{26}$$

where $Q_H(r,r',t)$ is given by Eq. (21) and $G_H(r,r',t)$ is defined by

$$G_H(r,r',t) = \int_0^t dt'[Q_H(r,r',t')\rho_H(t')\langle F_I(t)F_I(t')\rangle$$
$$- \rho_H(t')Q_H(r,r',t')\langle F_I(t')F_I(t)\rangle],\tag{27}$$

where $\langle F_I(t)F_I(t')\rangle$ and $\langle F_I(t')F_I(t)\rangle$ are the time correlation functions, for example,

$$\langle F_I(t)F_I(t')\rangle = \mathrm{Tr}_B[F_I(\{z_u\},t)F_I(\{z_u\},t')\rho_B(0)],\tag{28}$$

and a similar equation holds for $\langle F_I(t')F_I(t)\rangle$.

Equations (26) and (18) are the basic equations that have to be solved together. Since Eq. (26) depends through Eq. (27) on all previous times t', it contains memory, i.e., the equations of motion are non-Markovian. Equation (27) is evaluated by the trapezoidal rule.

For the model environment composed of harmonic oscillators [see Eq. (12)] it can be shown that

$$\langle F_I(t)F_I(t')\rangle = \frac{1}{2}\sum_u \frac{\hbar}{m_u\Omega_u}K_u^2\Phi(\Omega_u, t-t', T),\tag{29}$$

where

$$\Phi(\Omega_u, t-t', T) = \{[\bar{n}(\Omega_u)+1]\exp[-i\Omega_u(t-t')]$$
$$+ \bar{n}(\Omega_u)\exp[i\Omega_u(t-t')]\},\tag{30}$$

with the Bose-Einstein distribution function

$$\bar{n}(\Omega_u) = [\exp(\hbar\Omega_u/k_B T) - 1]^{-1},\tag{31}$$

and $\langle F_I(t)F_I(t')\rangle = \langle F_I(t')F_I(t)\rangle^*$.

As in the previous works [30,31] we set $(\hbar/m_u\Omega_u) = a_0^2$ in Eq. (29) and assume quasiresonant system-bath coupling represented by a Lorentzian-type function

$$g_{mn}(\Omega) = \frac{1}{\pi}(\gamma_{mn}/\Omega_0)^p \frac{\gamma_{mn}}{\gamma_{mn}^2 + (\omega_{mn} - \Omega)^2}, \qquad (32)$$

where $(\gamma_{mn}/\Omega_0)^p$ is a normalization factor, Ω_0 is a scaling parameter, $\gamma_{mn} > 0$ determines the width of the distribution $g_{mn}(\Omega)$, and ω_{mn} are the frequencies of the bound-bound transitions in OH. Further, in Eq. (29) we change from the infinite sum over u to a finite sum over $m > n$ containing integrals,

$$\langle F_I(t)F_I(t')\rangle = \frac{a_0^2}{2}\sum_u K_u^2 \Phi(\Omega_u, t - t', T)$$

$$\Rightarrow \frac{a_0^2}{2}\sum_{m=1}^{v_{max}}\sum_{n=0}^{m-1} K_{mn}^2 \int_{A_{mn}}^{B_{mn}} d\Omega\, \Phi(\Omega, t - t', T)g_{mn}(\Omega),$$

$$(33)$$

where $A_{mn} < \omega_{mn} < B_{mn}$. The distribution function $\bar{n}(\Omega_u)$ of Eq. (31) is approximated in each frequency domain $A_{mn} < \Omega < B_{mn}$ by its "central value" $\bar{n}(\omega_{mn})$. Assuming that the γ_{mn} in Eq. (32) can be chosen such that the neighboring distributions $g_{mn}(\Omega)$ do not overlap one another, we set $A_{mn} = -\infty$ and $B_{mn} = \infty$, which yields tabulated integrals [33] in Eq. (33). The final expression for the time correlation function of Eq. (29) reads

$$\langle F_I(t)F_I(t')\rangle = \frac{a_0^2}{2}\sum_{m=1}^{v_{max}}\sum_{n=0}^{m-1} K_{mn}^2(\gamma_{mn}/\Omega_0)^p e^{-\gamma_{mn}|t-t'|}\{[\bar{n}(\omega_{mn})$$

$$+ 1]e^{-i\omega_{mn}(t-t')} + \bar{n}(\omega_{mn})e^{i\omega_{mn}(t-t')}\}, \qquad (34)$$

where v_{max} is the the number of the topmost vibrational bound state of OH, i.e., $v_{max} = 21$. Further, a particular system-bath coupling is specified by the parameters K_{mn}, γ_{mn}, Ω_0, and p. Here we adapt the model used in [30,31] and set $K_{mn}^2 = \delta_{mk}\delta_{nl}$, $p = 1$, $\Omega_0 = \omega_{10}$, and $\gamma_{mn} = (\Delta^a/2)$. Δ^a is the anharmonicity constant of OH, defined from the difference between the Morse (ω_{10}) and the harmonic (ω_H) fundamental frequencies, $\Delta^a = -(\omega_{10} - \omega_H)/2$. Thus, within the present model, all that is needed is ω_{10} and Δ^a.

Equations (18) and (26) were represented on equidistant two-dimensional grids at grid points r_i and r_i'. We used 1024×1024 grid points from $r_{min} = 0.05a_0$ to $r_{max} = 87.41a_0$ for the r and r' variables. Equation (18) was propagated with the split-operator technique with the time step $\Delta t = 4$ atomic time units (a.t.u.). Spatial derivatives $\partial^2 S(r, r', t)/\partial r^2$ in Eq. (18) were calculated with the DF2TCF and DF2TCB routines of IMSL. At large values of the internuclear distance r, the outgoing part of the time-evolution operator $S(t)$ was damped by a time-dependent imaginary optical potential

$$V_{opt}(r \ge r_{opt}, t) = -i\Upsilon(t)V_0 \exp\left[\frac{3}{2}\left(1 - \frac{(r_{max} - r_{opt})^2}{(r - r_{opt})^2}\right)\right],$$

$$(35)$$

and $V_{opt}(r < r_{opt}, t) = 0$. The time-independent part of the optical potential is adopted from [34]; see also references therein. The smooth switching term $\Upsilon(t)$ is chosen such as to avoid absorption of the ingoing evolution operator $S(t)$. Specifically, $\Upsilon(t < t_1) = 0$,
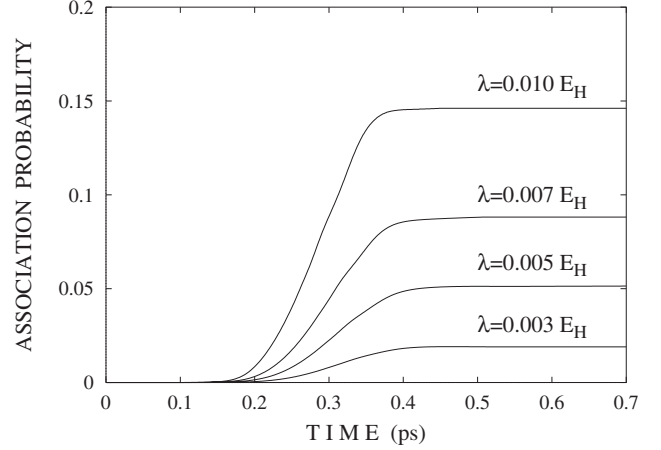
FIG. 1. Laser-free association of OH in a quasiresonant bath at $T = 300$ K. The association probability is calculated as the total population of all bound states of OH. The strengths of the system-bath couplings λ, defined by Eq. (37), are given near the corresponding curves.

$$\Upsilon(t_1 \le t \le t_2) = \sin^2\left[\frac{\pi}{2}\left(\frac{t - t_1}{t_2 - t_1}\right)\right], \qquad (36)$$

and $\Upsilon(t > t_2) = 1$. The results presented in the next section have been calculated with $t_1 = 0.3$ ps, $t_2 = 0.4$ ps, $V_0 = 0.055E_H$, and $r_{opt} = 80.72a_0$. Equation (26) was propagated with the well known predictor-corrector method, as in our previous work [29–31].

III. ASSOCIATION OF OH

The initial state of the O+H collision, specified by Eqs. (22), (8), and (7), corresponds to the center of mass collision energy of $E_c = 0.355 \times 10^{-2}E_H$, which is a typical order of magnitude for atomic beam experiments. The initial energy E_c is a suitable reference for the strength of the system-bath coupling, which will be defined therefore by a parameter

$$\lambda = \Lambda a_0^2, \qquad (37)$$

with the dimension of energy. The temperature of the bath is assumed to be $T = 300$ K. The association probability is calculated as the total population of all bound states of OH, i.e.,

$$P_{as} = \sum_{v=0}^{v_{max}} \rho_{vv}(t). \qquad (38)$$

A. The laser-free association

The time-dependent laser-free association of OH resulting from an inelastic collision of O and H atoms is illustrated in Fig. 1 for four different strengths of the system-bath coupling λ. The values of the system-bath coupling λ in Fig. 1 approximately correspond to the numbers of association "channels" efficiently "opened" to the initial state of the O+H system with the initial collision energy of E_c. At $\lambda = 0.003E_H$ for example, the energy difference $E_c - E_{v=21} = 0.368 \times 10^{-2}E_H$ is slightly larger than the system-bath cou-

(a)

(b)
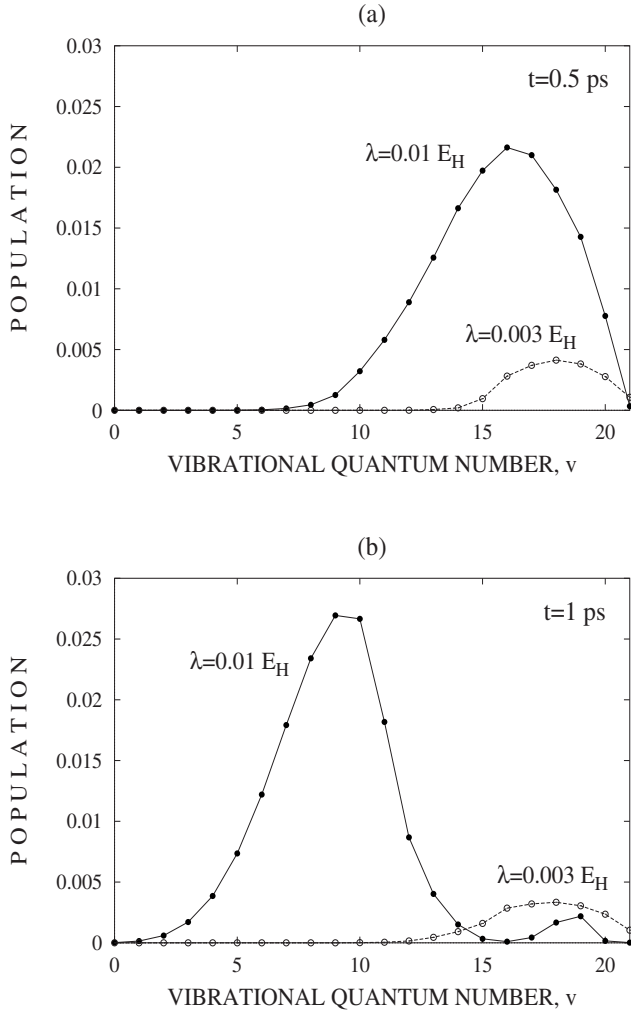
FIG. 2. Populations of vibrational bound states of OH at $t=$(a) 0.5 and at (b) 1 ps versus the vibrational quantum number v for two system-bath couplings: $\lambda=0.01E_H$ (solid lines) and $0.003E_H$ (dashed lines).

pling, and therefore only one association channel (via the topmost bound state $|v=21\rangle$) is opened. At $\lambda=0.005E_H$, the lower bound state $|v=20\rangle$ is also involved: $E_c-E_{v=20}=0.457\times10^{-2}E_H<\lambda$, and one more association channel is opened. Similarly, additional association channels, via states $|v=19\rangle$ and $|v=18\rangle$, are opened at $\lambda=0.007E_H$ and $0.01E_H$, respectively. Therefore, at large couplings association starts earlier and proceeds with a higher rate than at small ones. At $t>0.5$ ps, when the colliding O and H atoms leave the interaction domain, the association probability reaches saturation.

Populations of the vibrational bound states of OH at $t=0.5$ and at 1 ps are shown in Fig. 2 versus the vibrational quantum number at a weak system-bath coupling $\lambda=0.003E_H$ (one association channel is opened initially) and at a strong coupling $\lambda=0.01E_H$ (four association channels are opened). At $t=0.5$ ps, when association reaches the saturation domain and the total population of the bound states does not change (see Fig. 1), only high-lying vibrational states of OH are populated substantially, as is seen from Fig. 2(a). The maximum population corresponds to the state $|v=18\rangle$ at the weak system-bath coupling of $\lambda=0.003E_H$ and to the state

$|v=16\rangle$ at the strong coupling of $\lambda=0.01E_H$. At a later time, $t=1$ ps [Fig. 2(b)], the lower bound states of OH are being populated at the expense of the higher ones. At the small coupling $\lambda=0.003E_H$, the distribution of populations becomes more flat, although the maximum population is still at $v=18$. Much lower vibrational states have dominant populations at $t=1$ ps in the case of the strong coupling $\lambda=0.01E_H$.

Figure 2 thus demonstrates the effect of vibrational relaxation of highly excited OH on a picosecond time scale. One recognizes the (trivial) effect that vibrational relaxation is the faster the larger the coupling parameter λ. A nontrivial observation is that, in the case of the strong coupling $\lambda=0.01E_H$, for example, the overall distribution of populations is still very far from equilibrium at $t=1$ ps, including the existence of two ensembles: "cold" with a maximum at $v=9$ and "hot" with a maximum at $v=19$. The bimodal distribution observed at $t=1$ ps and $\lambda=0.01E_H$ suggests that not only "downward" $|v\rangle\rightarrow|v-1\rangle$ but also "upward" $|v\rangle\rightarrow|v+1\rangle$ transitions took place, because after $t=0.5$ ps the reflected part of the wave packet left the interaction region and the association probability remained constant according to Fig. 1.

B. The laser-driven association

Next we study the laser-pulse assisted state-selective association of OH. Here, the interaction of the O+H system with the bath can play a dual role in the laser-driven association. On the one hand, the probability of the laser-driven association can be increased due to the system-bath coupling which results in association even without a laser field, as discussed above. On the other hand, the laser-free association reduces the norm of the unbound part of the initial wave function, thus reducing the probability of the state-selective laser-driven association to be addressed below.

For the latter, we choose the bound state $|v=15\rangle$ of OH as the intermediate target and start with the investigation of the resonant association with the laser frequency of $\omega=(E_c-E_{v=15})/\hbar$, implying the one-photon laser-driven association pathway

$$|E_c\rangle\rightarrow|v=15\rangle+\hbar\omega. \tag{39}$$

The vector potential $A(t)$ in the system-field interaction Hamiltonian $\hat{H}_{SF}$ of Eq. (5) is chosen in the following form:

$$A(t)=\frac{c}{\omega}\mathcal{E}_0\sin^2(\pi t/t_p)\cos(\omega t+\varphi), \tag{40}$$

where $\mathcal{E}_0$ is the amplitude, $t_p=0.5$ ps is the pulse duration at the base, ω is the laser carrier frequency, and φ is the phase. In what follows, the case of $\varphi=0$ is considered, and the electric field $\mathcal{E}(t)=-(1/c)\partial A(t)/\partial t$ is given by

$$\mathcal{E}(t)=\mathcal{E}_0\left(\sin^2(\pi t/t_p)\sin(\omega t)-\frac{\pi}{\omega t_p}\sin(2\pi t/t_p)\cos(\omega t)\right). \tag{41}$$

The first term in Eq. (41) corresponds to a $\sin^2$-shaped laser pulse, while the second, the so-called switching term, ap-
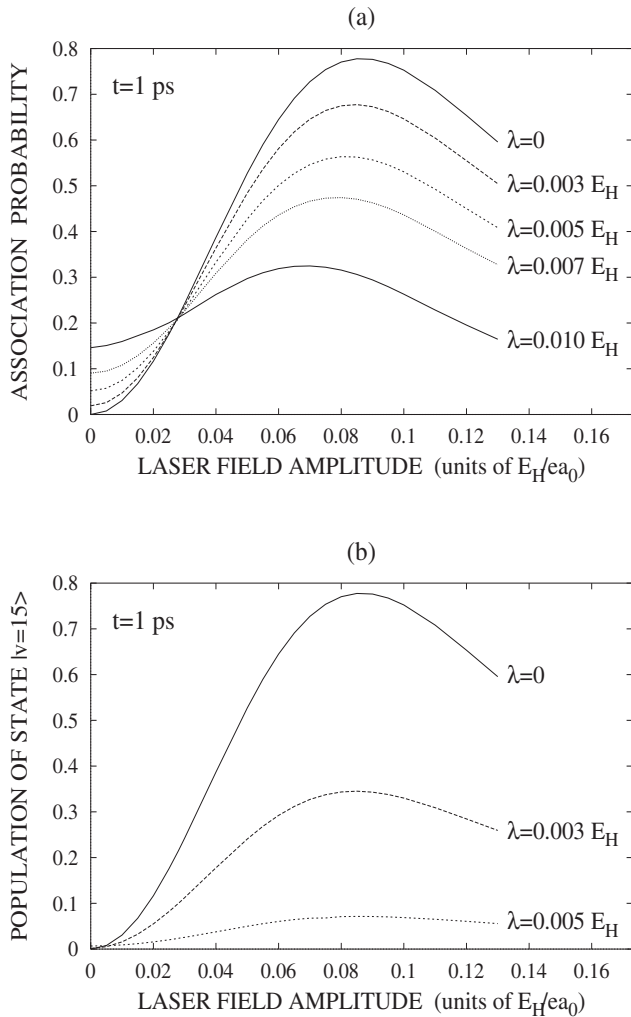
FIG. 3. Laser-driven association of OH in a quasiresonant bath at $T = 300$ K. The association probability (a) and the population of the "pumped" state $|v = 15\rangle$ (b) at $t = 1$ ps versus the amplitude of the resonant laser pulse. The laser pulse parameters are $t_p = 0.5$ ps, $\omega = 0.021\,26 E_H / \hbar$.

pears due to the finite pulse duration [35,36]. The definition of the electric field via the vector potential, suggested in [35], assures that the electric field has a vanishing direct-current (dc) component, $\int_0^{t_p} \mathcal{E}(t) dt = 0$, and satisfies the Maxwell equations in the propagation region.

The association probabilities and populations of the intermediate target state $|v = 15\rangle$ of OH at $t = 1$ ps are shown in Figs. 3(a) and 3(b), respectively, versus the amplitude $\mathcal{E}_0$ of the 0.5 ps laser pulse with the resonant carrier frequency of $\omega = 0.021\,26 E_H / \hbar$ corresponding to the photoassociation pathway (39). The time interval of 1 ps includes the 0.5 ps laser-driven association followed by 0.5 ps of free evolution. The strengths of the system-bath couplings λ are indicated at the respective curves, the case of $\lambda = 0$ is also included for comparison.

From Fig. 3(a) the following observations are made.

(i) A maximum of the association probability occurs at a certain field amplitude, for each of the curves.

(ii) The system-bath coupling can play a dual role with respect to the efficiency of the laser-driven association. At

relatively weak laser fields, $\mathcal{E}_0 < 0.029 E_H / ea_0$ in the case of OH under study, the association probability is increased due to the system-bath coupling and strong couplings are preferable for efficient association. In contrast, in stronger laser fields, $\mathcal{E}_0 > 0.029 E_H / ea_0$, the association probability is higher for smaller system-bath couplings, and weak system-bath couplings are preferable for the efficient association.

(iii) It is very interesting that all five curves in Fig. 3(a), corresponding to five different system-bath couplings, cross at the same "isosbestic" point which corresponds to the pulse amplitude of $\mathcal{E}_0 \approx 0.029 E_H / ea_0$. At this isosbestic value of the laser-pulse amplitude, $\mathcal{E}_0 = \mathcal{E}_0^i$, the probability of the laser-driven association of OH in an environment does not depend on the strength of the system-bath coupling at all.

(iv) The maxima in Fig. 3(a) which correspond to optimal field strengths are shifted toward the isosbestic point as the system-bath coupling λ gets larger.

The occurrence of an isosbestic point for the multilevel OH system of course does not mean that the same population of bound states occurs at this point, rather the sum of the bound state populations is the same. This is indicated in Fig. 3(b), which shows the population of the laser-pumped state $|v = 15\rangle$ at $t = 1$ ps. The population of the pumped state $|v = 15\rangle$ is almost equal to the overall association probability if $\lambda = 0$, and decreases drastically with the increase of the system-bath coupling λ. At $\lambda > 0.005 E_H$ it is so small as to be neglected. The latter observations are due to the fast vibrational relaxation to lower bound states. At the isosbestic field strength $\mathcal{E}_0$, the population of state $|15\rangle$ is different for different λ, and consequently also the populations of other states must be different for different dissipative coupling. For $\lambda \neq 0$, the bound state populations are also time dependent.

One of the most interesting effects is the counterintuitive decrease of the association probability with increasing system-bath coupling λ at strong laser fields $\mathcal{E}_0 > \mathcal{E}_0^i$ [see Fig. 3(a)]. Possible reasons for the decreased association probability are as follows. A strong laser field dumps more and more energy into the molecule and thus heats it up. Moreover, if the laser field gets too strong it becomes no longer optimal for the chosen continuum-bound transition at a given laser frequency and the pulse duration. Finally, a strong coupling to the bath broadens the laser-pumped state $|v = 15\rangle$ into a resonance such that the laser frequency is no longer optimal for the respective transition. An intuitive expectation that increasing the coupling to the bath would help the molecule cool off is fully realized after the end of a strong laser pulse: the population of the pumped state $|v = 15\rangle$ strongly decreases with the increase of the system-bath coupling λ [see Fig. 3(b)] due to a fast relaxation to the lower-lying vibrational states of OH [see Fig. 5(a) in the next section].

Before analyzing the results for OH further, we note that the observations in Fig. 3(a) are quite generic. In fact, the main findings (i)–(iv) can be explained by a simple Markovian two-state model. In this model, an initially occupied, high-energy state $|1\rangle$ is resonantly coupled by a $\sin^2$ pulse to a low-energy state $|0\rangle$. To make contact with the OH problem, state $|1\rangle$ is assumed to have a certain lifetime $\tau = \Gamma^{-1}$ (where Γ is the dissipative transition rate from $|1\rangle$ to $|0\rangle$) and is interpreted as the "continuum state" with energy E_c as above. State $|0\rangle$ is a model for a bound, associative state, e.g.,
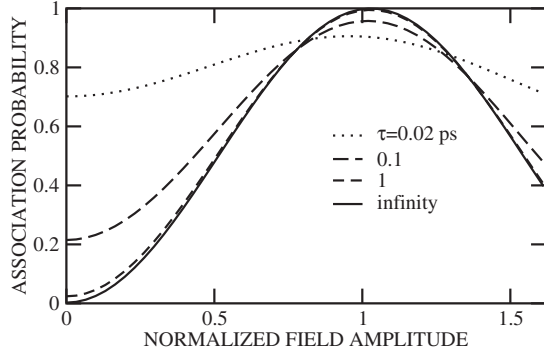
FIG. 4. Association probability as a function of normalized field amplitude for a two-level system (see text). The lifetime of the initial state, $\tau = \Gamma^{-1}$, is indicated.

the acceptor state $|v=15\rangle$ as above. We assume a certain dipole coupling μ_{10} between the two states, an energy difference of $\hbar\omega_{10}=0.02E_H$, and a pulse of the form (41) with duration $t_p=0.5$ ps and carrier frequency $\omega=\omega_{10}$. The total propagation time was 1 ps as above. The Markovian equations of motion for the diagonal elements of the density operator are

$$\frac{d\rho_{11}}{dt} = -\frac{i}{\hbar}\mathcal{E}(t)(\mu_{10}\rho_{01}-\rho_{10}\mu_{01}) - \Gamma\rho_{11}, \qquad (42)$$

$$\frac{d\rho_{00}}{dt} = -\frac{i}{\hbar}\mathcal{E}(t)(\mu_{01}\rho_{10}-\rho_{01}\mu_{10}) + \Gamma\rho_{11}, \qquad (43)$$

where ρ_{01} and ρ_{10} are coherences for which similar equations of motion exist. Solving these equations with the initial condition $\rho_{11}(0)=1$ for different field amplitudes $\mathcal{E}_0$ and τ gives for the population of state $|0\rangle$ after 1 ps (the "association probability") the curves shown in Fig. 4.

It is found that Fig. 3(a) is qualitatively reproduced, with the following interpretation.

(i) The maximum is due to a first Rabi maximum, corresponding to a π pulse. A π pulse leads to a perfect population inversion in a dissipation-free two-level system. For a $\sin^2$ pulse, one finds the condition $\mu_{10}\mathcal{E}_0 t_p/2\hbar=\pi$. Therefore, when plotting the *normalized field amplitude* $\mathcal{E}_0' = \mu_{10}\mathcal{E}_0 t_p/2\pi\hbar$ as abscissa the π pulse maximum occurs at $\mathcal{E}_0'=1$, which is well satisfied in Fig. 4. Further maxima occur in Fig. 4 (not shown) for $\mathcal{E}_0'=3,5,7,\dots$, and minima for $\mathcal{E}_0' =0,2,4,\dots$. In the dissipation-free case, $\Gamma=0$, the oscillation(s) in Fig. 4 is (are) between $\rho_{00}=0$ and $\rho_{00}=1$.

(ii) If dissipation is present, $\Gamma>0$, the amplitude of oscillation is damped with enhanced association probability at low fields $\mathcal{E}_0$, and a reduced yield around the maximum. The enhancement at low $\mathcal{E}_0$ is due to the fact that even for a vanishing field there is association due to fast relaxation. Dissipation also explains why the level inversion is incomplete around the maximum, similar to the limited yield one obtains for the inverse process, photon absorption.

(iii) An isosbestic point around $\mu_{10}\mathcal{E}_0 t_p/2\hbar \approx 0.8\pi$ marks the transition between the two regimes. From Fig. 4 we note, however, two refinements relative to Fig. 3: First, for very fast dissipation [$\Gamma=(0.02\ \text{ps})^{-1}$] the ρ_{00} curves move out of

phase, i.e., the corresponding curve no longer goes through $\mathcal{E}_0^i$. Second (for not too strong dissipation), there is a second isosbestic point beyond the maximum at high field strengths, basically for symmetry reasons.

Note that the counterintuitive decrease of the association probability with increasing coupling parameter λ for strong fields is reproduced within the simple two-state model, at least in the interval $\mathcal{E}_0^{i1}<\mathcal{E}_0<\mathcal{E}_0^{i2}$, where $\mathcal{E}_0^{i1}$ and $\mathcal{E}_0^{i2}$ denote the two isosbestic points. It is a simple consequence of the damped Rabi oscillations: Increasing λ lifts the minima and lowers the maxima. Of course, the two-state model is too simple to reproduce the precise behavior indicated in Fig. 3. In particular, no second isosbestic point is found in Fig. 3 for field strengths up to $0.14E_H/ea_0$.

(iv) The (first) maximum of the $\rho_{00}(\mathcal{E}_0)$ curves shifts to lower field strength as Γ becomes larger. This can be understood from the extreme case of very large Γ. Then, after 1 ps all the population has already decayed to state $|0\rangle$ even at $\mathcal{E}_0=0$. Thus, ρ_{00} is maximal at $\mathcal{E}_0=0$ and finite fields can only diminish ρ_{00}. If, on the other hand, Γ is zero, the maximum of ρ_{00} is at the Rabi field amplitude.

We extended our investigation to a three-state model (with a continuum state $|2\rangle$ above $|1\rangle$), and also to various Markovian multistate models and to slightly off-resonant laser fields. As a result, the *qualitative* observations (i)–(iv) remain valid, showing again that a substantial part of the physics contained in Fig. 3(a) can be mapped onto an effective, dissipative two-level system. Quantitative details such as the nonoccurrence of a second isosbestic point in Fig. 3(a) are absent in generic few-level models and require a system-specific treatment.

C. Optimal control of OH association

Returning to OH, we note that the dependence of the association probability on the amplitude of the laser pulse shown in Fig. 3(a) provides the first step of the overall optimization of the laser pulse aimed to maximize the association yield at a given system-bath coupling λ. Further optimizations of the laser carrier frequency and the laser pulse amplitude make it possible to substantially increase the association probability, by more than 20%. Association dynamics of OH controlled by the optimal 0.5 ps laser pulse at a "moderate" system-bath coupling of $\lambda=0.005E_H$ is illustrated in Fig. 5(a) with the time-dependent association probability and populations of several bound vibrational states of OH, including the pumped state $|v=15\rangle$, which acquire significant population on the time interval of 1 ps. The optimal laser field is shown in Fig. 5(b). For the sake of comparison, we show in Fig. 5(c) the association dynamics of OH controlled by the optimal 0.5 ps laser pulse at $\lambda=0$ [the optimal pulse shown in Fig. 5(d)].

It is seen from Fig. 5(a) that the association probability reaches the saturation domain at $t\approx0.45$ ps and does not change at a later time. Up to 60% of population is localized in the pumped state $|v=15\rangle$ at $t\approx0.4$ ps. At a later time, the population of $|v=15\rangle$ state decreases due to vibrational relaxation to the lower bound states, which facilitates the stabilization of OH in the ground electronic state. The maximal
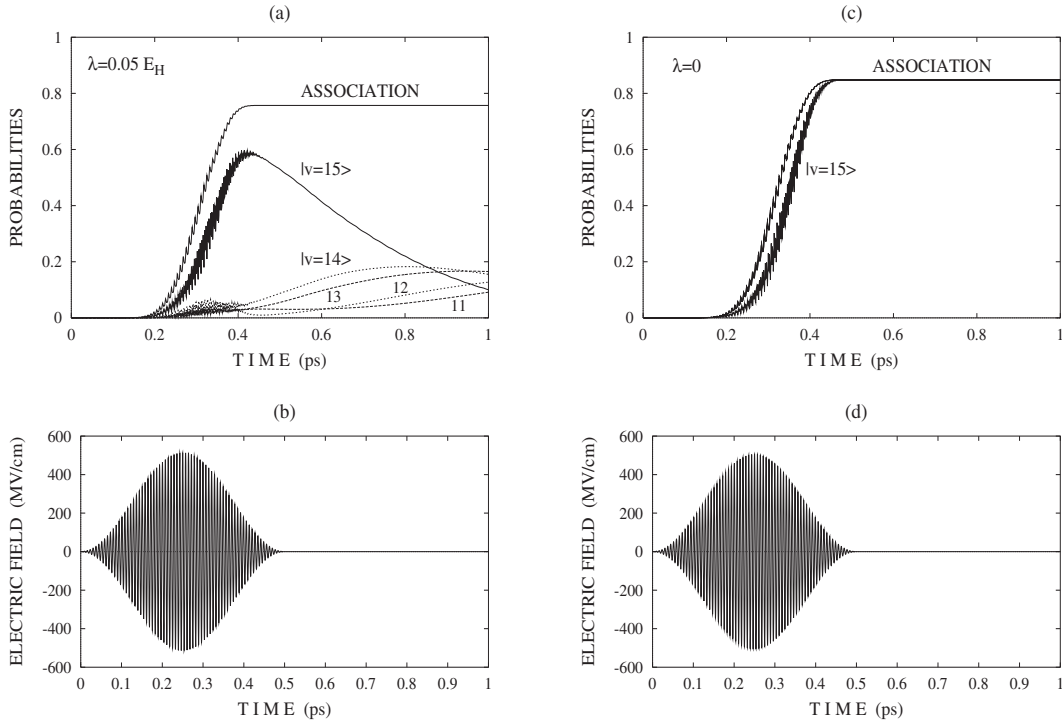
FIG. 5. Association of OH by the optimal 0.5 ps laser pulses. (a) Time-dependent association probability and populations of the bound states of OH at $\lambda=0.005E_H$ and $T=300$ K. (b) The optimal laser pulse: $t_p=0.5$ ps, $\mathcal{E}_0=0.0999E_H/ea_0$, $\omega=0.021\,51E_H/\hbar$. (c) Time-dependent association probability and population of the target state $|v=15\rangle$ at $\lambda=0$. (d) The optimal laser pulse: $t_p=0.5$ ps, $\mathcal{E}_0=0.0984E_H/ea_0$, $\omega=0.021\,42E_H/\hbar$.

association probability of 0.757, obtained at $\lambda=0.005E_H$ with the optimal laser frequency $\omega=0.021\,51E_H/\hbar$ [Fig. 5(a)], is higher by more than 20% than that obtained with the resonant frequency $\omega=0.021\,26E_H/\hbar$ at the same system-bath coupling [Fig. 3(a)], but smaller by about 10% as compared to the maximal association probability obtained at $\lambda=0$ [Fig. 5(c)]. The reason for the latter is that at $\lambda=0.005E_H$, the optimal pulse amplitude $\mathcal{E}_0=0.0999E_H/ea_0$ is larger than the isosbestic field strength $\mathcal{E}_0^i\approx0.029E_H/ea_0$ [see Fig. 3(a)] and the association probability is smaller as compared to the case of $\lambda=0$ [see Fig. 5(c)].

Note that the association dynamics shown in Fig. 5(c) at $\lambda=0$ is very similar to that presented in our previous work [8] (see Fig. 2 therein) except that the maximal association probability of 0.848 obtained in the present work is slightly higher than the maximal probability of 0.846 obtained in [8], where the photoassociation of OH was studied without dissipation within the Schrödinger wave-function formalism. The reason for this small difference is that the optimal laser field obtained in the present work is slightly different from that of the previous work [8], where the switching term in Eq. (41) was not included.

IV. CONCLUSIONS

The time-evolution operator method used in the present work is well known and widely used in the derivation of general equations of motion; see, for example, [32]. The time-evolution operator method is also very suitable for isolated systems in the Schrödinger wave-function formalism: if

the time-evolution operator is known, one can easily evaluate the quantum dynamics of the system under study at any initial conditions. On the other hand, the time-evolution operator method can be too expensive in the Schrödinger wave-function formalism, because it doubles the dimensionality of the problem under consideration: instead of propagating, e.g., a one-dimensional wave function, one should propagate the two-dimensional time-evolution operator. In contrast, in the density matrix formalism the dimensionality of the problem to be solved numerically is not changed if the time-evolution operator is employed, and one can substantially simplify the corresponding equations of motion by making use of it.

In the present work, the time-evolution operator method was applied to the closed-system part of the overall time-dependent Hamiltonian, which made it possible to transform the open-system equation of motion to the Heisenberg picture suitable for the numerical propagation. Numerical implementation for the association reaction $O+H\rightarrow OH$ revealed that the system-bath coupling can play a dual role with respect to the efficiency of the laser-driven association: the association probability is increased due to the system-bath coupling if the laser field strength is smaller than the isosbestic value $\mathcal{E}_0=\mathcal{E}_0^i$, but decreased if the field strength is greater than $\mathcal{E}_0^i$. If the field strength is equal to the isosbestic value $\mathcal{E}_0=\mathcal{E}_0^i$, the association probability does not depend on the strength of the system-bath coupling at all. In the case of the association reaction $O+H\rightarrow OH$, studied in this work, the optimal field strength maximizing the association probability is greater than the isosbestic field strength of $\mathcal{E}_0^i$

$\approx 0.029 E_H/ea_0$, and the association probability is decreased as the system-bath coupling is increased.

Note, finally, that the difference between the results obtained with the zero-area (present work) and nonzero-area (previous work [8]) laser pulses is very small because the number of optical cycles per the pulse duration at the base, $t_p=0.5$ ps, is more than 70 and the switching term in Eq. (41) is of minor importance. If the number of optical cycles per pulse duration is small enough, the aforementioned difference is quite substantial. Moreover, with the number of optical cycles being less than 15, the phase of the laser field starts to play an important role as well (see, e.g., [38]), and one should always take into account that the area of the laser pulse used in the numerical simulations must vanish [37]. The definition of the electric field via the vector potential,

suggested in Ref. [35], assures that the area of the pulse is zero. The other way to handle this problem is the use of an integer number of optical cycles at the base of the pulse. With a symmetric envelope of the pulse, such as the $\sin^2$ envelope for example, the area of the pulse is always equal to zero, although the pulse duration at the base t_p depends on the laser carrier frequency.

ACKNOWLEDGMENTS

[1] H. R. Thorsheim, J. Weiner, and P. S. Julienne, Phys. Rev. Lett. **58**, 2420 (1987).

[2] P. D. Lett, K. Helmerson, W. D. Phillips, L. P. Ratliff, S. L. Rolston, and M. E. Wagshul, Phys. Rev. Lett. **71**, 2200 (1993).

[3] M. Machholm, A. Giusti-Suzor, and F. H. Mies, Phys. Rev. A **50**, 5025 (1994).

[4] C. J. Williams and P. S. Julienne, J. Chem. Phys. **101**, 2634 (1994).

[5] L. P. Ratliff, M. E. Wagshul, P. D. Lett, S. L. Rolston, and W. D. Phillips, J. Chem. Phys. **101**, 2638 (1994).

[6] Y. B. Band and P. S. Julienne, Phys. Rev. A **51**, R4317 (1995).

[7] U. Marvet and M. Dantus, Chem. Phys. Lett. **245**, 393 (1995).

[8] M. V. Korolkov, J. Manz, G. K. Paramonov, and B. Schmidt, Chem. Phys. Lett. **260**, 604 (1996).

[9] H. M. J. M. Boesten, C. C. Tsai, B. J. Verhaar, and D. J. Heinzen, Phys. Rev. Lett. **77**, 5194 (1996).

[10] P. Backhaus, J. Manz, and B. Schmidt, Adv. Chem. Phys. **101**, 86 (1997).

[11] M. V. Korolkov and B. Schmidt, Chem. Phys. Lett. **272**, 96 (1997).

[12] P. Backhaus, B. Schmidt, and M. Dantus, Chem. Phys. Lett. **306**, 18 (1999).

[13] M. Mackie and J. Javanainen, Phys. Rev. A **60**, 3174 (1999).

[14] J. Vala, O. Dulieu, F. Masnou-Seeuws, P. Pillet, and R. Kosloff, Phys. Rev. A **63**, 013412 (2000).

[15] C. P. Koch, J. P. Palao, R. Kosloff, and F. Masnou-Seeuws, Phys. Rev. A **70**, 013402 (2004).

[16] E. Luc-Koenig, R. Kosloff, F. Masnou-Seeuws, and M. Vatasescu, Phys. Rev. A **70**, 033414 (2004).

[17] K. M. Jones, E. Tiesinga, P. D. Lett, and P. S. Julienne, Rev. Mod. Phys. **78**, 483 (2006).

[18] Y. Niu, S. Wang, and S. Cong, Chem. Phys. Lett. **428**, 7 (2006).

[19] E. F. de Lima and J. E. M. Hornos, Chem. Phys. Lett. **433**, 48

(2006).

[20] C. P. Koch, R. Kosloff, and F. Masnou-Seeuws, Phys. Rev. A **73**, 043409 (2006).

[21] E. Luc-Koenig, F. Masnou-Seeuws, and R. Kosloff, Phys. Rev. A **76**, 053415 (2007).

[22] M. Nest and H.-D. Meyer, J. Chem. Phys. **119**, 24 (2003).

[23] W. Brenig, Phys. Scr. **35**, 329 (1987).

[24] B. Jackson, Comput. Phys. Commun. **80**, 119 (1994).

[25] P. Saalfrank, J. Chem. Phys. **113**, 3780 (2000).

[26] M. Nest and P. Saalfrank, J. Chem. Phys. **113**, 8753 (2000).

[27] S. Gao, J. Strömquist, and B. I. Lundqvist, Phys. Rev. Lett. **86**, 1805 (2001).

[28] P. Saalfrank and R. Kosloff, J. Chem. Phys. **105**, 2441 (1996).

[29] G. K. Paramonov, S. Beyvers, I. Andrianov, and P. Saalfrank, Phys. Rev. B **75**, 045405 (2007).

[30] M. V. Korolkov and G. K. Paramonov, Phys. Rev. A **55**, 589 (1997).

[31] M. V. Korolkov and G. K. Paramonov, Phys. Rev. A **56**, 3860 (1997).

[32] K. Blum, *Density Matrix Theory and Applications* (Plenum, New York, 1989).

[33] I. S. Gradshteyn and I. M. Ryzhik, *Table of Integrals, Series, and Products* (Academic, New York, 1980).

[34] M. Kaluža, J. T. Muckerman, P. Gross, and H. Rabitz, J. Chem. Phys. **100**, 4211 (1994).

[35] A. D. Bandrauk and N. H. Shon, Phys. Rev. A **66**, 031401(R) (2002).

[36] N. Došlić, Phys. Rev. A **74**, 013402 (2006).

[37] A. D. Bandrauk, S. Barmaki, S. Chelkowski, and G. L. Kamta, in *Progress in Ultrafast Intense Laser Science III*, edited by K. Yamanochi, S. L. Chin, P. Agostini, and G. Ferrante, Springer Series in Chemical Physics Vol. 84 (Springer, Berlin, 2008), pp. 171–206.

[38] K.-M. Weitzel, ChemPhysChem **8**, 213 (2007).